Supporting information for

Microparticle separation using asymmetrical induced-charge electro-osmotic vortices on an arc-edge-based floating electrode

Xiaoming Chen[1], Yukun Ren[*1,2,3], Likai Hou[1], Xiangsong Feng[1], Tianyi Jiang[1], and Hongyuan Jiang[*1,2]

1. School of Mechatronics Engineering, Harbin Institute of Technology, Harbin 150001, PR China
2. State Key Laboratory of Robotics and System, Harbin Institute of Technology, Harbin 150001, PR China
3. State Key Laboratory of Nonlinear Mechanics, Chinese Academy of Sciences, Beijing 100190, PR China

Section 1: Induced-charge electro-osmotic flow in focusing and separation region

When the over-potential is small, we can ignore steric effect and non-uniform surface conduction on the floating electrode. For this, the classic induced-charge electro-osmosis (ICEO) model can be used to descript the microstream on the conductor surface. The induced double layer (IDL) on the conductor surface is treated as tandem surface capacitor, and it's capacitance can be expressed as:[1]

$$C_0 = \frac{C_d C_s}{C_d + C_s} = \frac{1}{1+\delta} C_d \tag{S1}$$

where, $C_d = \frac{\varepsilon_f}{\lambda_d}$ is the capacitance of diffusion layer (ε_f and λ_d the permittivity and Debye screening length of electrolyte respectively). C_s is the capacitance of stern layer. $\delta = \frac{C_d}{C_s}$ is the a surface capacitance ratio.

Since the conductivity in the buffer solution is uniform, the electrostatic potential in the microchannel is governed by Laplace equation:

$$\nabla^2 \phi = 0 \tag{S2}$$

We consider the interface of conductor and electrolyte as an interfacial capacitance and provide interfacial jump condition to describe the IDL.

$$\sigma \cdot \boldsymbol{n} \nabla \tilde{\phi} = j\omega C_0 \left(\tilde{\phi} - \tilde{\phi}_0 \right) \tag{S3}$$

where, σ is the conductivity of buffer solution, $\omega = 2\pi f$ is the angular field frequency. $\tilde{\phi}$ and $\tilde{\phi}_0$ are the potential in the bulk and on the floating electrode, respectively.

In the focusing and separation region, the voltage drops across diffuse layer actuate ICEO flow on their floating electrode:

$$\tilde{\zeta}^1 = \frac{1}{1+\delta}\left(\tilde{\phi}_0^{\,1} - \tilde{\phi}^1 \right) \tag{S4}$$

$$\tilde{\zeta}^2 = \frac{1}{1+\delta}\left(\tilde{\phi}_0^{\,2} - \tilde{\phi}^2 \right) \tag{S5}$$

The tangential electric field exerts Coulomb force on the excessive counterions within the diffuse screening cloud.[2, 3]

$$\boldsymbol{E}^1_t = \mathrm{Re}\left(\tilde{\boldsymbol{E}}^1_t e^{j\omega_1 t} \right) = \mathrm{Re}\left(\left(\tilde{\boldsymbol{E}}^1 - \tilde{\boldsymbol{E}}^1 \cdot \boldsymbol{n} \cdot \boldsymbol{n} \right) e^{j\omega_1 t} \right) \tag{S6}$$

$$\boldsymbol{E}^2_t = \mathrm{Re}\left(\tilde{\boldsymbol{E}}^2_t e^{j\omega_2 t} \right) = \mathrm{Re}\left(\left(\tilde{\boldsymbol{E}}^2 - \tilde{\boldsymbol{E}}^2 \cdot \boldsymbol{n} \cdot \boldsymbol{n} \right) e^{j\omega_2 t} \right) \tag{S7}$$

The motion of counterions producing nonlinear electroosmotic slip velocity on two floating electrodes.

$$\left\langle \boldsymbol{u}_{slip}{}^1 \right\rangle = \frac{\varepsilon}{2\eta(1+\delta)} \mathrm{Re}\left(\left(\tilde{\phi}^1 - \tilde{\phi}_0^{\,1} \right) \left(\boldsymbol{E}_1 - \boldsymbol{E}_1 \cdot \boldsymbol{n} \cdot \boldsymbol{n} \right)^* \right) \tag{S8}$$

$$\left\langle \boldsymbol{u}_{slip}{}^2 \right\rangle = \frac{\varepsilon}{2\eta(1+\delta)} \mathrm{Re}\left(\left(\tilde{\phi}^2 - \tilde{\phi}_0^{\,2} \right) \left(\boldsymbol{E}_2 - \boldsymbol{E}_2 \cdot \boldsymbol{n} \cdot \boldsymbol{n} \right)^* \right) \tag{S9}$$

Inserting the equation (S8) and (S9) into full Stokes equation as a boundary condition to calculate the bulk ICEO flow field in the focusing and separation region.

$$\nabla \cdot \boldsymbol{u} = 0 \tag{S10}$$

$$-\nabla p + \eta \nabla^2 \boldsymbol{u} = 0 \tag{S11}$$

Section 2: Dielectrophoresis

Because light and small particles are elevated to higher level from channel bottom and arc-shape side wall of floating electrode in separation region will generate electric field gradient, dielectrophoretic (DEP) force plays a non-ignorable role in particle behaviors. DEP force acting on the surface induced charge drives particle with the higher/ lower polarizability than the buffer solution to get close/away from the side wall of floating electrode. The DEP force for a sphere particle with a radius *r* is given by:[4]

$$\left\langle \boldsymbol{F}_{DEP} \right\rangle = \pi \varepsilon_f r^3 \,\mathrm{Re}\left(f_{CM}\right) \nabla \left(\tilde{E} \cdot \tilde{E}^* \right) \tag{S12}$$

where, r is the radius of particle, $\mathrm{Re}(f_{CM})$ the CM factor of particle.

Section 3: Particle motion in the channel

Under the effect of gravity, electric and flow field, particle travels in the channel with the velocity:[5]

$$\begin{aligned} \boldsymbol{u}_p &= \boldsymbol{u}_{Inlet} + \boldsymbol{u}_{buoyancy} + \boldsymbol{u}_{DEP}{}^1 + \boldsymbol{u}_{DEP}{}^2 + \boldsymbol{u}_{ICEO}{}^1 + \boldsymbol{u}_{ICEO}{}^2 \\ &= \boldsymbol{u}_{Inlet} + \boldsymbol{u}_{ICEO}{}^1 + \boldsymbol{u}_{ICEO}{}^2 - \frac{2r^2}{9\eta}\left(\rho_p - \rho_f\right) g \boldsymbol{e}_z + \frac{\varepsilon_f r^2}{6\eta}\left[\mathrm{Re}\left(f'_{CM}\right) \nabla \left(\tilde{\boldsymbol{E}}_1 \cdot \tilde{\boldsymbol{E}}_1^* \right) + \mathrm{Re}\left(f''_{CM}\right) \nabla \left(\tilde{\boldsymbol{E}}_2 \cdot \tilde{\boldsymbol{E}}_2^* \right) \right] \end{aligned} \tag{S13}$$

where, $\boldsymbol{u}_{Inlet}$ is the inlet fluid flow, $\boldsymbol{u}_{ICEO}{}^1$ and $\boldsymbol{u}_{ICEO}{}^2$ are the velocity induced by electric field 1 and 2. $\mathrm{Re}(f'_{CM})$ and $\mathrm{Re}(f''_{CM})$ the CM factor of particle in AC electric field 1 and 2. We can get the particle trajectory in the channel by integrating its velocity about travel time *t*.

Section 4: Definition of focusing width and deflection.

Fig. S1 illustrates the motion of particle stream, schematically. We defined two indexes, focusing width *W* and deflection *D*, to establish an AICEO characterization of the particles.

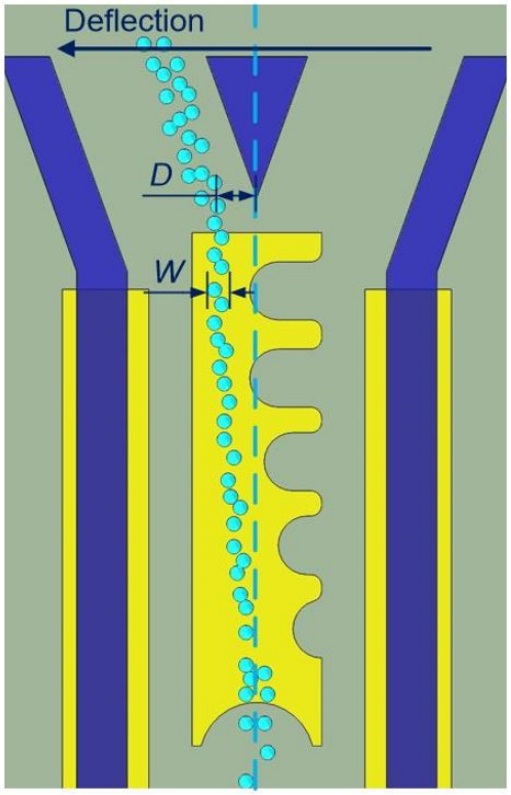

Fig. S1. Diagram depicting the behaviors of particles in the separation region and defining the focusing width *W* and deflection *D*. (the navy arrow aligns with the positive direction of deflection).

Section 5: Simulation analyzing the effect of gap shape on the AICEO transverse flow rate

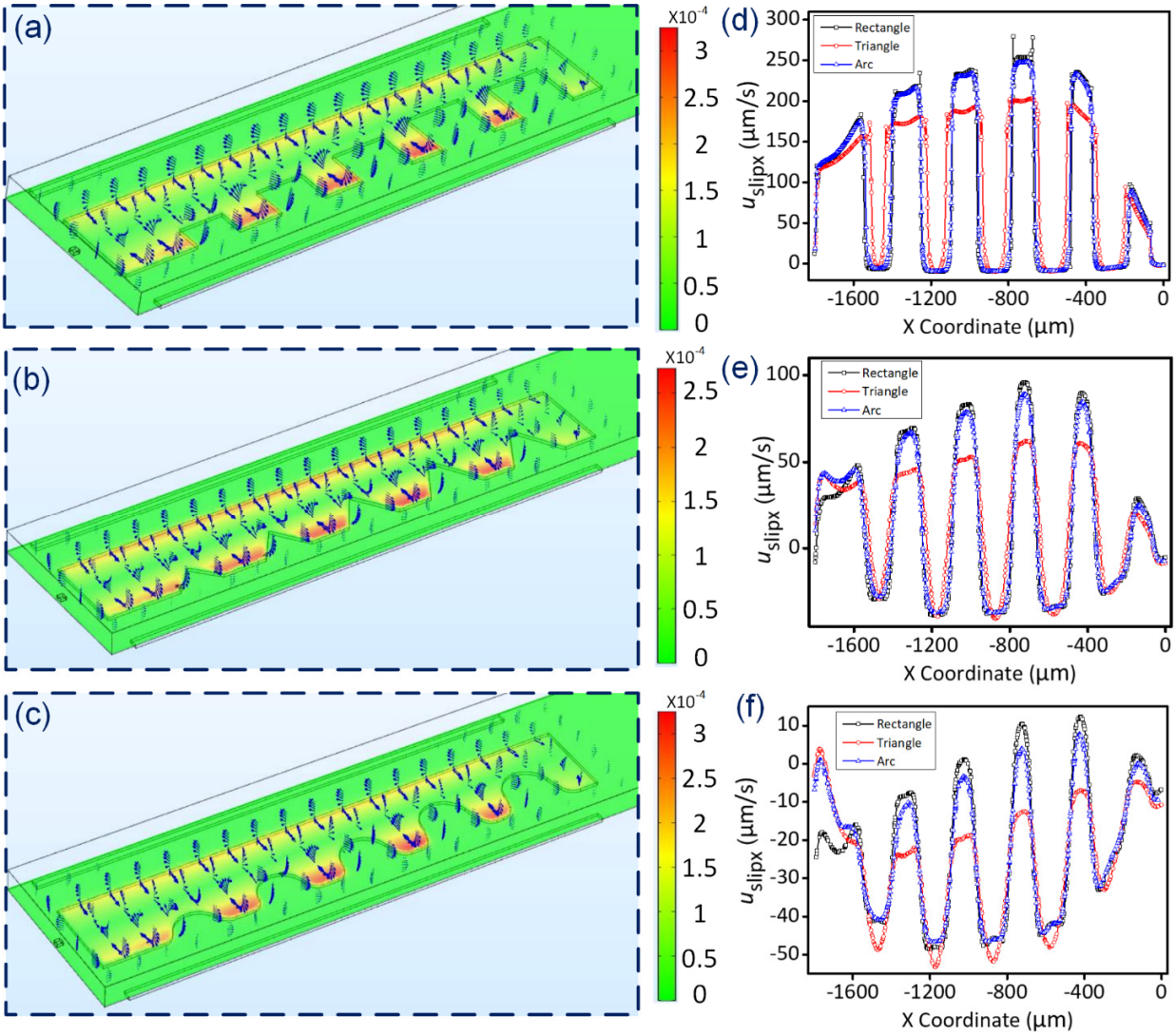

Fig. S2 Simulation analyzing the effect of gap shape the asymmetrical ICEO (AICEO) transverse flow rate along the cutting line. (Cutting line with the distance 90 μm to the channel centerline on the x-y plane 1, 2, 3. Plane 1, 2, 3 with the distance 4, 21, 36 μm to the floating electrode, respectively.) (a-c) The floating electrode with rectangle, triangle and arc gaps inducing spatial vortices distribution in the channel. (d-f) The transverse flow rate along the cutting line on the plane 1, 2, 3 for different shape gaps of floating electrode. (d) Rectangle. (e) Triangle. (f) Arc.

In the process of device design, we compared the velocity distributions on the floating electrode with rectangle, triangle and arc gaps to determine the reasonable structure. The spatial vortices distribution of the floating electrode with rectangle/ triangle/ arc gaps is given Fig.S2 a/ b/ c. Evidently, compared to the floating electrode with rectangle and arc gaps, the vortices induced by triangle-gap-shaped floating electrode have relative lower transverse flow rate. On the plane 1, the transvers velocity induced by rectangle-gap-shaped side wall is largest but with obvious sudden change. Although the transverse velocity caused by the triangle-gap-shaped side wall has a broad range, it has low velocity magnitude with clear fluctuation at the triangle edge of floating electrode. To our satisfaction, the transverse

velocities induced by arc- and rectangle-gap-shaped side wall is comparable. More importantly, the transverse velocity has no fluctuation at the arc edge (Fig. S2d). The transverse flow rate follow the cutting line on the x-y plane 2/ 3 for the floating electrode with the rectangle, triangle and arc gaps are presented in Fig. S2 e/ f. Similarly, on plane 2 and 3, the transverse velocities on the floating electrode with arc gaps have large magnitude and no fluctuation at the edge. Therefore, we chose the arc-shape-based floating electrode to generate AICEO vortices in the device design.

Section 6: Device fabrication[6, 7]

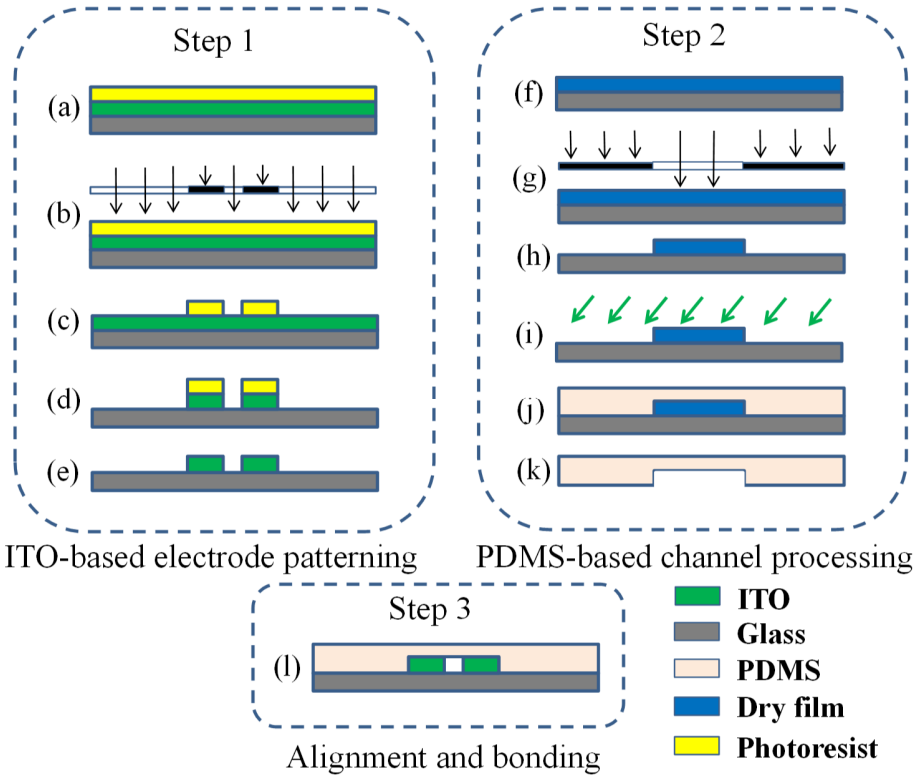

Fig. S3. A schematic diagram illustrating the device fabrication. (a) Positive photoresist (AZ4620) was coated on the glass substrate with ITO film at the speed of 3000 rad/min and baked at 100°C for 6 minutes; (b) Positive photoresist was exposed under the UV light to obtain designed electrode structure; (c) Exposed positive resist film is processed in the developer (ZX-238) and baked at 110 °C for 6 minutes; (d) The substrate with positive resist film was submerged in etching solution to gain the electrode; (e) Positive photoresist is removed from the ITO-based electrode in the (NMP EL); (f) Two

layers of dry film (Riston SD238, Dupont, USA) were laminated on the clean glass; (g) Dry film was exposed under the UV light to obtain desired mold structure; (h) Exposed dry film was processed in the $NaHCO_3$ solution to get the channel mold. (i) After baking treatment at 50 °C for 6 minutes, the mold was treated with 1H, 1H, 2H, 2H-perfluorooctyltrichlorosilane (Sigma Aldrich, USA) to reduce its surface energy. (j) PDMS is casted with dry-film mold; (k) PDMS channel was peeled off from the mold; (l) The ITO-based electrode and PDMS-based channel were aligned and bonded under the microscope after a surface treatment of oxygen plasma.

Section 7: Micrographs of uniform-sized and multi-sized yeast cells

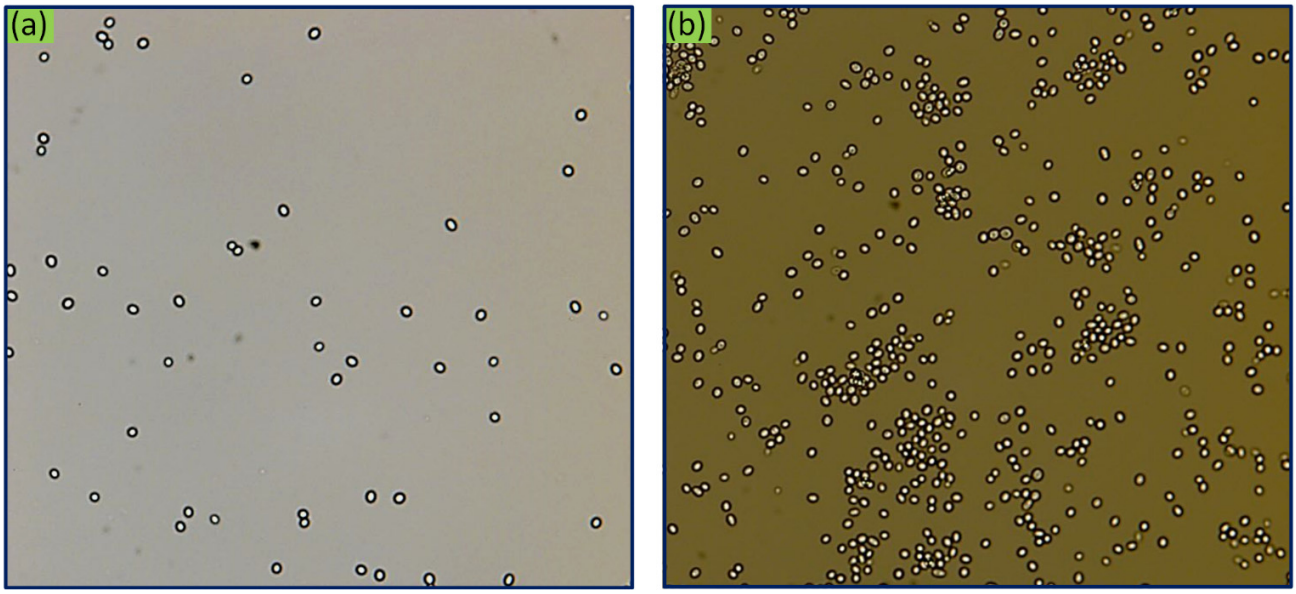

Fig. S4. Micrographs of yeast cells. (a) Uniform-sized yeast cells. (b) Multi-sized yeast cells

Section 8: Actual photographs illustrating the AICEO characterization of cells and particles

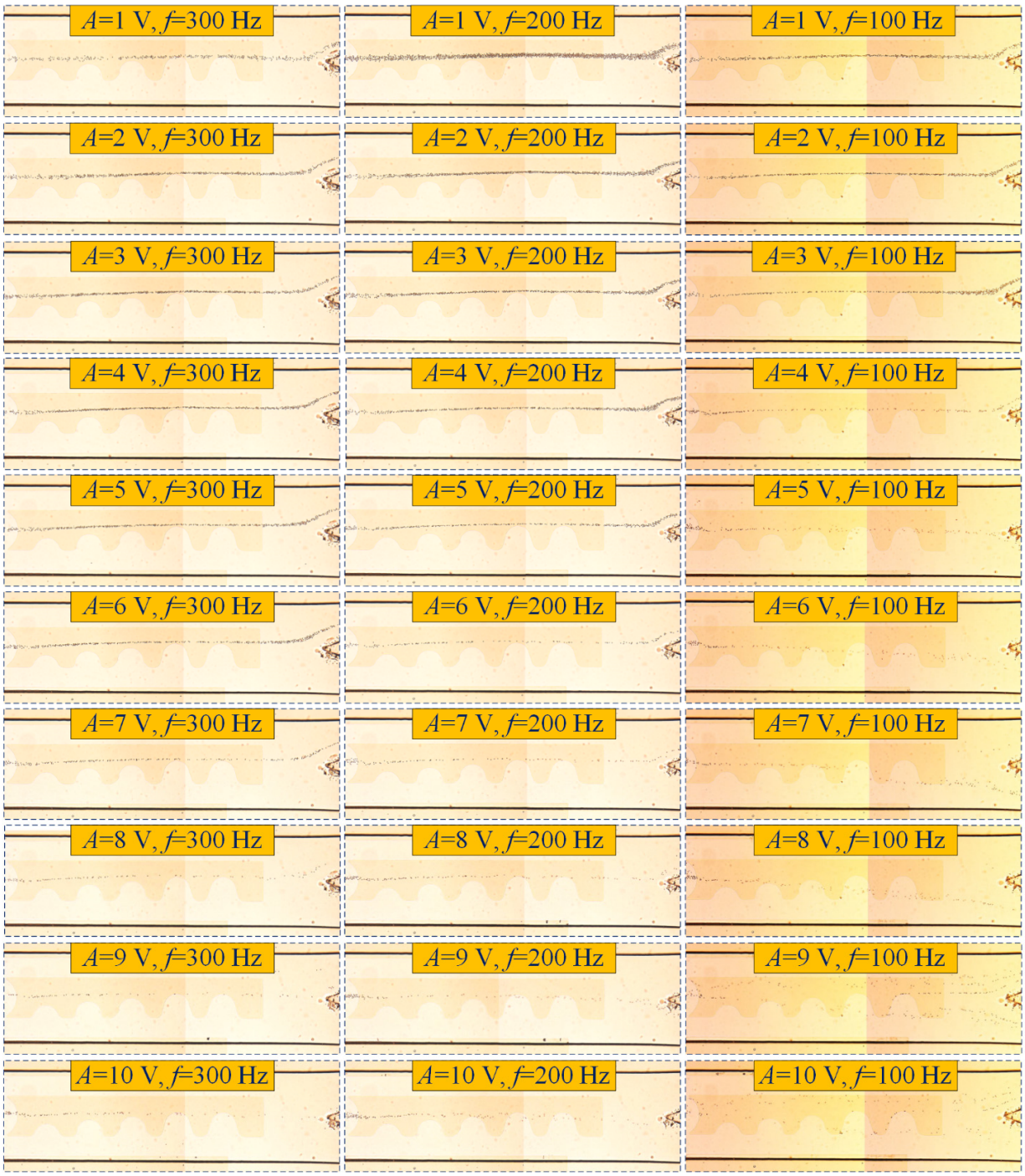

Fig. S5. Actual microphotographs of Polymethyl Methacrylate (PMMA) particle focusing and deflection under different voltage frequencies and intensities.

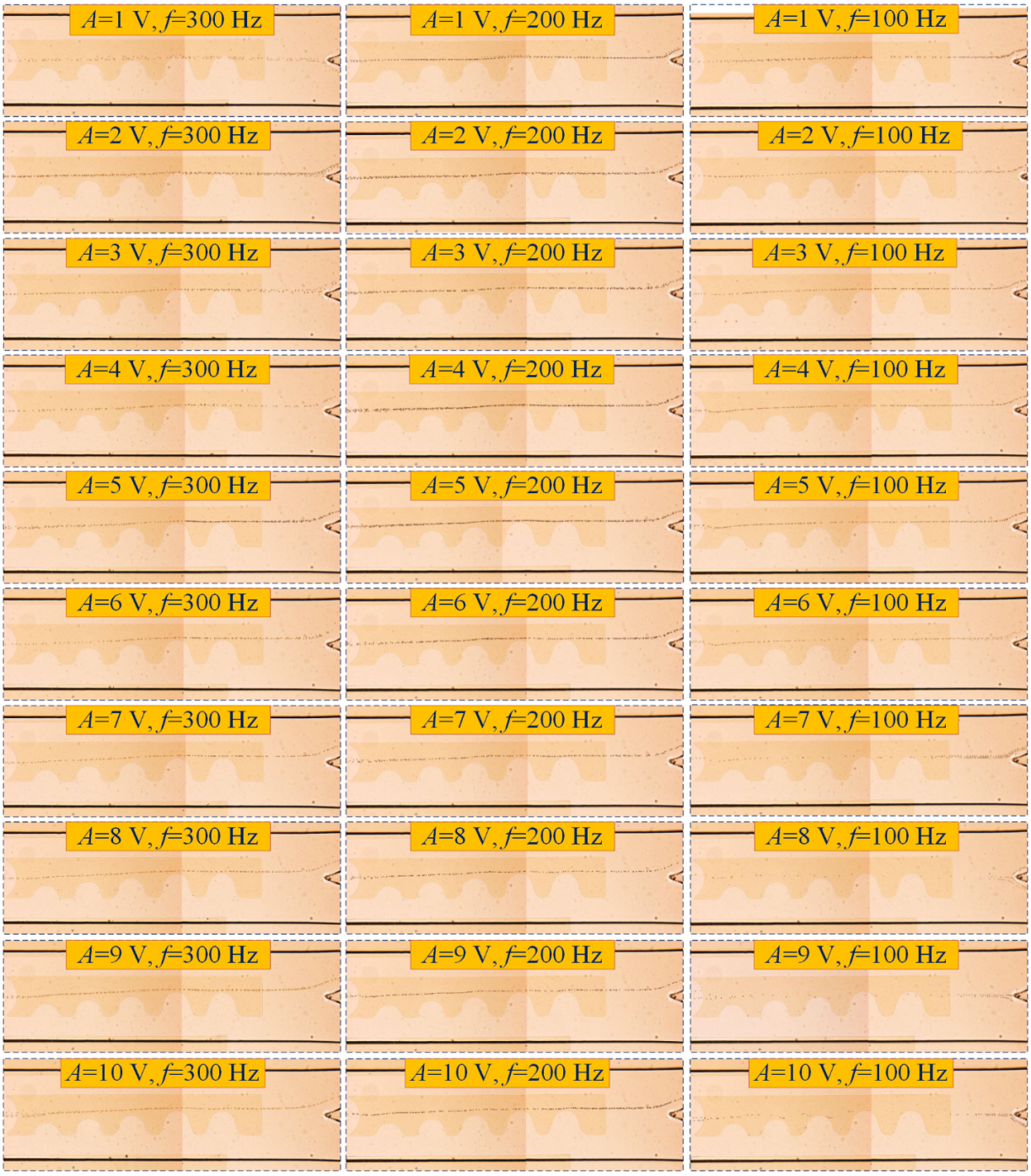

Fig. S6. Actual microphotographs of silica particle focusing and deflection under different voltage frequencies and intensities.

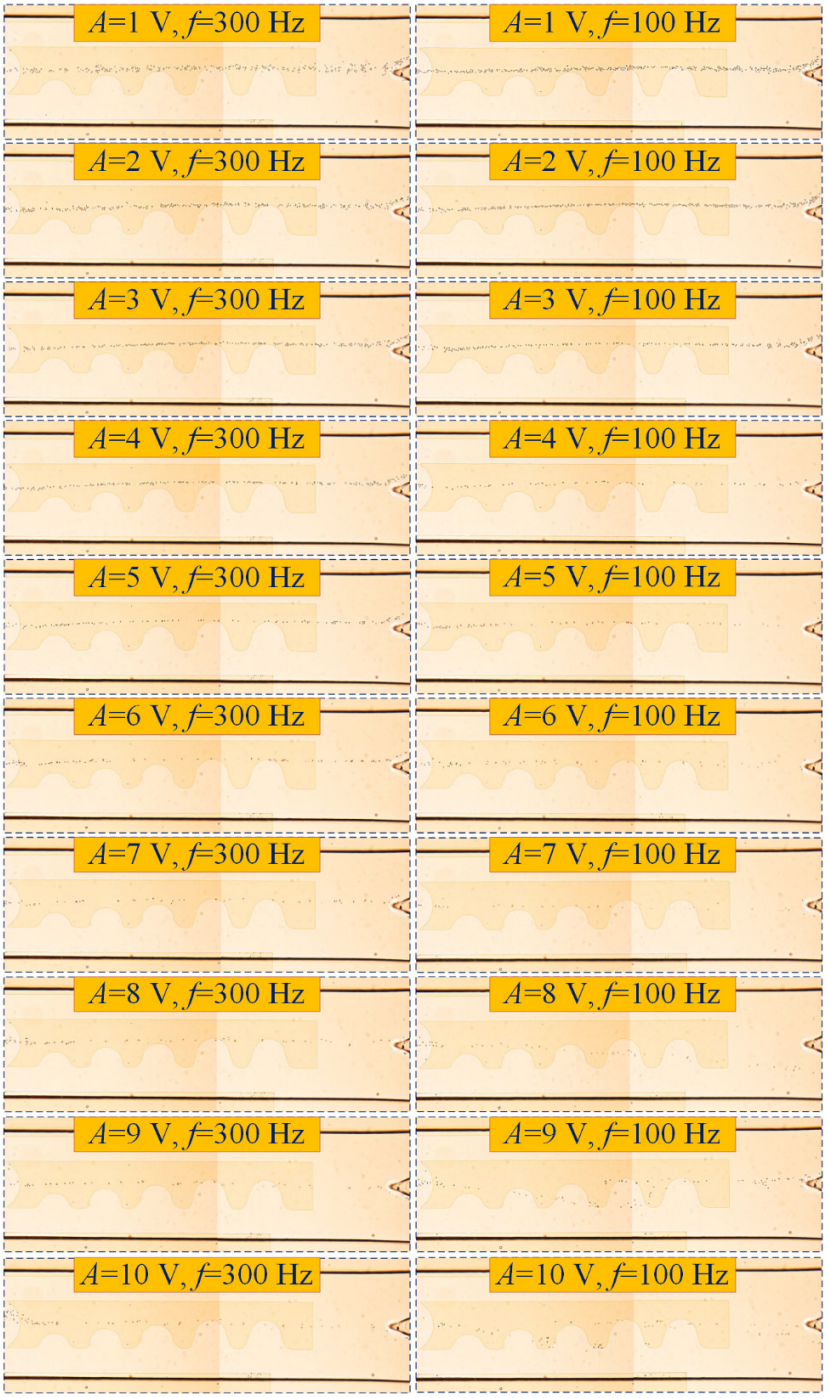

Fig. S7. Actual microphotographs of uniform-sized yeast cell focusing and deflection under different voltage frequencies and intensities.

Section 9: Supplementary Movies

Movie S1 Separation of 4-μm PMMA and 4-μm silica particles at f_1=100 Hz, A_1=3 V, f_2=100 Hz, A_2=9 V and u=28.8 μL/h

Movie S2 Separation of multi-sized yeast cells at f_1=200 Hz, A_1=4 V, f_2=100 Hz, A_2=5 V and u=28.8 μL/h

Movie S3 Separation of uniform-sized yeast cells and 4-μm silica particles at f_1=100 Hz, A_1=3 V, f_2=100 Hz, A_2=7 V and u=28.8 μL/h

References

1. T. M. Squires and M. Z. Bazant, *Journal of Fluid Mechanics*, 2004, **509**, 217-252.
2. Y. Ren, W. Liu, Y. Jia, Y. Tao, J. Shao, Y. Ding and H. Jiang, *Lab on a chip*, 2015, **15**, 2181-2191.
3. Y. Ren, W. Liu, J. Liu, Y. Tao, Y. Guo and H. Jiang, *Biomicrofluidics*, 2016, **10**, 054103.
4. N. Lewpiriyawong, K. Kandaswamy, C. Yang, V. Ivanov and R. Stocker, *Analytical chemistry*, 2011, **83**, 9579-9585.
5. Y. Ren, X. Liu, W. Liu, Y. Tao, Y. Jia, L. Hou, W. Li and H. Jiang, *Electrophoresis*, 2018, **39**, 597-607.
6. X. Chen, Y. Ren, W. Liu, X. Feng, Y. Jia, Y. Tao and H. Jiang, *Analytical chemistry*, 2017, **89**, 9583-9592.
7. Y. Jia, Y. Ren and H. Jiang, *RSC Advances*, 2015, **5**, 66602-66610.